

Extending Sequential Leaching Approaches to Stable Sr Isotopes in Carbonate Reference Materials

Jena Jeong,^{a,b,*} Seung-Gu Lee,^a and Youngsook Huh^{b,*}

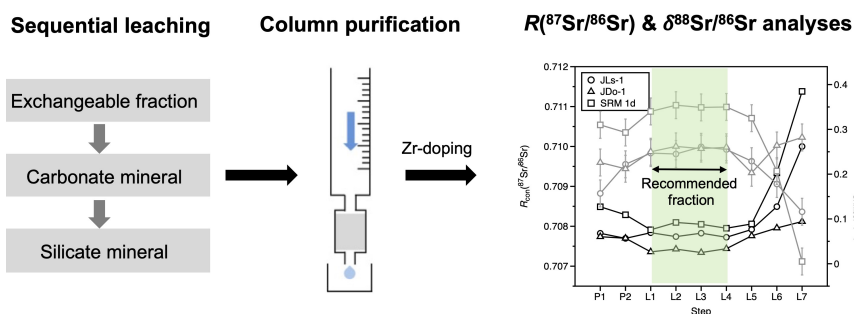
^aGeological Survey Division, Korea Institute of Geoscience and Mineral Resources, Daejeon 34132, South of Korea

^bSchool of Earth and Environmental Sciences, Seoul National University, Seoul 08826, Republic of Korea

Received: February 09, 2026; Revised: April 06, 2026; Accepted: April 06, 2026; Available online: April 06, 2026.

DOI: 10.46770/AS.2026.012

ABSTRACT: Reliable Sr isotope analysis of carbonate rocks requires effective separation of non-carbonate phases that can bias both radiogenic ($R(^{87}\text{Sr}/^{86}\text{Sr})$) and stable ($\delta^{88}\text{Sr}/^{86}\text{Sr}_{\text{SRM987}}$) isotope measurements. While sequential leaching has been evaluated using the $R(^{87}\text{Sr}/^{86}\text{Sr})$, the behavior of $\delta^{88}\text{Sr}/^{86}\text{Sr}_{\text{SRM987}}$ during this process remains poorly constrained. Here, we systematically investigate the evolution of both radiogenic and stable Sr isotopes across sequential leaching steps in three carbonate reference materials, JLS-1, JDo-1, and NIST SRM 1d. This study reports new $\delta^{88}\text{Sr}/^{86}\text{Sr}_{\text{SRM987}}$ data for individual leaching fractions of carbonate reference materials and provides the first sequential leaching-based Sr isotope dataset for NIST SRM 1d, for which both radiogenic and stable Sr isotope data have previously been limited. Early leaching fractions are dominated by surface-adsorbed and exchangeable Sr, whereas later fractions reflect contributions from clay minerals, both of which produce isotopic signatures distinct from primary carbonate phases. Only intermediate fractions yield reproducible Sr isotope compositions representative of primary carbonate minerals. The $R(^{87}\text{Sr}/^{86}\text{Sr})$ values obtained from bulk leaching differ from those of the intermediate fractions by more than analytical precision, whereas smaller but detectable effects ($\sim 0.03\%$) are observed for $\delta^{88}\text{Sr}/^{86}\text{Sr}_{\text{SRM987}}$, especially in clay-rich samples. Applying the carbonate-dominated leaching range, representative values of carbonate reference materials are obtained with $R(^{87}\text{Sr}/^{86}\text{Sr})$ of 0.707783 ± 0.000028 , 0.707386 ± 0.000028 , and 0.708008 ± 0.000028 , and $\delta^{88}\text{Sr}/^{86}\text{Sr}_{\text{SRM987}}$ of $0.252 \pm 0.035\%$, $0.256 \pm 0.035\%$, and $0.325 \pm 0.035\%$ for JLS-1, JDo-1 and SRM 1d, respectively (2SD). These results demonstrate that not only $R(^{87}\text{Sr}/^{86}\text{Sr})$ but also $\delta^{88}\text{Sr}/^{86}\text{Sr}_{\text{SRM987}}$ are sensitive to phase-specific Sr released during leaching and highlight the necessity of accurate pretreatment for Sr isotope analysis. The dataset and analytical framework presented here expand the application of sequential leaching method and improve the utility of carbonate reference materials for high-precision isotope studies.



INTRODUCTION

Carbonate rocks are valuable archives of ancient seawater chemistry and environmental evolution, as their direct precipitation from marine waters preserves the isotopic composition of past oceans. Among the diverse geochemical signals preserved in these carbonates, radiogenic strontium isotope ratio ($R(^{87}\text{Sr}/^{86}\text{Sr})$) has long been used to reconstruct changes in

the major fluxes that govern the evolution of seawater chemistry.^{1–3} Owing to its long residence time of roughly 2.5 Myr, Sr exhibits a homogeneous isotopic composition in modern seawater and behaves as a conservative trace element.⁴ Variations in the seawater $R(^{87}\text{Sr}/^{86}\text{Sr})$ values over geological time reflect large-scale processes such as continental weathering, seafloor hydrothermal activity, and volcanic outgassing, providing a robust proxy for global tectonic and climatic evolution.^{1,5} Through decades of accumulated research, a well-resolved global seawater

$R(^{87}\text{Sr}/^{86}\text{Sr})$ curve has been established across geological time, allowing Sr isotopes to serve as a powerful tool for chemostratigraphic studies.^{3,6}

Over the past 20 years, analytical advances in mass spectrometry have expanded Sr isotope studies beyond radiogenic $R(^{87}\text{Sr}/^{86}\text{Sr})$ to include stable isotope variations expressed as $\delta^{88}\text{Sr}/^{86}\text{Sr}_{\text{SRM987}}$, defined by:

$$\delta^{88}\text{Sr}/^{86}\text{Sr}_{\text{SRM987}} (\text{‰}) = \left(\frac{\left(\frac{^{88}\text{Sr}}{^{86}\text{Sr}} \right)_{\text{sample}}}{\left(\frac{^{88}\text{Sr}}{^{86}\text{Sr}} \right)_{\text{SRM987}}} - 1 \right) \times 1000 \quad (1)$$

where SRM 987 is an international standard from the National Institute of Standards and Technology (NIST). Stable Sr isotopes ($\delta^{88}\text{Sr}/^{86}\text{Sr}_{\text{SRM987}}$) constitute a powerful non-traditional geochemical proxy, particularly effective when integrated with the $R(^{87}\text{Sr}/^{86}\text{Sr})$ for reconstructing paleoenvironmental conditions and the long-term evolution of Earth's geochemical cycle.^{7,8} Unlike the radiogenic Sr isotope system, which primarily reflects the relative magnitude and composition of input fluxes (e.g., continental weathering and hydrothermal activity), $\delta^{88}\text{Sr}/^{86}\text{Sr}_{\text{SRM987}}$ value is sensitive to variations in the ocean Sr output flux dominated by marine carbonate burial.^{7,9,10} This difference arises from mass-dependent fractionation during carbonate precipitation, where the preferential incorporation of lighter Sr isotopes yields lower $\delta^{88}\text{Sr}/^{86}\text{Sr}_{\text{SRM987}}$ values in carbonate minerals relative to seawater.^{9–11} Critically, the magnitude of Sr isotope fractionation has a negative correlation with the rate of mineral precipitation, allowing $\delta^{88}\text{Sr}/^{86}\text{Sr}_{\text{SRM987}}$ to function as a novel proxy for tracking the evolution of marine carbonate chemistry and saturation states through geologic time.^{8,11,12} The lack of correlation between $\delta^{88}\text{Sr}/^{86}\text{Sr}_{\text{SRM987}}$ and $R(^{87}\text{Sr}/^{86}\text{Sr})$ over most of the Phanerozoic further indicates that these isotope systems are governed by distinct mechanisms, providing complementary constraints for evaluating past changes in continental weathering and global carbonate burial rates.^{7,8}

Obtaining the primary seawater signal preserved in marine carbonates is essential for reconstructing paleoenvironments. However, natural carbonate rocks often contain non-carbonate minerals such as Fe–Mn oxyhydroxides, clay minerals, and secondary calcite, which can host Sr with isotopic compositions different from those of the primary carbonate minerals.^{13–15} Even minor contributions from these phases can distort the original seawater signal.^{15–17} Consequently, sequential leaching methods have been widely developed to separate contaminant phases from primary carbonate.^{14–18}

Previous studies have shown that $R(^{87}\text{Sr}/^{86}\text{Sr})$ can vary markedly throughout the leaching steps, reflecting the progressive dissolution of distinct mineral phases during sequential extraction. A typical sequential leaching method for carbonate rocks involves

an initial pre-leaching step using ammonium acetate.^{14,19} Sequential leaching experiments conducted on both limestones and dolostones suggest that $R(^{87}\text{Sr}/^{86}\text{Sr})$ values obtained from the ammonium acetate fraction can differ by up to ~ 0.004 from those of subsequent leaching steps.^{14,20–22} These results indicate that the pre-leaching step effectively removes exchangeable or surface-adsorbed Sr, as well as secondary calcite present in bulk rocks. Following this pre-leaching step, primary carbonate minerals are progressively dissolved using acetic acid or dilute hydrochloric acid. However, as dissolution proceeds into later stages, partial dissolution of silicate minerals introduces Sr with isotopic compositions distinct from those of primary carbonate.^{14,15} Samples with higher clay mineral contents exhibit large shifts in $R(^{87}\text{Sr}/^{86}\text{Sr})$ toward the final leaching steps.^{14,18,20} Collectively, these findings highlight the importance of careful leaching procedures for obtaining reliable Sr isotopic data from both limestones and dolostones.

Despite the extensive body of work on $R(^{87}\text{Sr}/^{86}\text{Sr})$, systematic investigations of $\delta^{88}\text{Sr}/^{86}\text{Sr}_{\text{SRM987}}$ behavior during sequential leaching remain limited. Importantly, experimental and natural studies indicate that primary rock dissolution does not induce significant mass-dependent Sr isotope fractionation. Instead, minor isotopic differences observed between leachates and residual solids, particularly in silicate rocks, are generally attributed to mineralogical heterogeneity rather than fractionation during dissolution itself.^{23–25} This implies that the Sr isotope composition of a given leachate primarily reflects the isotopic signature of the specific phase being dissolved at each step. Consistent with this interpretation, previous study has shown that bulk leaching with acids of varying strength may result in small but detectable differences in $\delta^{88}\text{Sr}/^{86}\text{Sr}_{\text{SRM987}}$ values in carbonate standards JLS-1 (limestone), implying that individual leaching steps may possess distinct stable Sr isotope compositions.²⁶ In addition, several studies have suggested that variability in $\delta^{88}\text{Sr}/^{86}\text{Sr}_{\text{SRM987}}$ among samples may influence $R(^{87}\text{Sr}/^{86}\text{Sr})$ values through internal normalization.^{27–29} This implies that accurate determination of $\delta^{88}\text{Sr}/^{86}\text{Sr}_{\text{SRM987}}$ is important not only for stable Sr isotope studies but also for ensuring the reliability of radiogenic Sr isotope measurements. However, detailed sequential leaching experiments examining $\delta^{88}\text{Sr}/^{86}\text{Sr}_{\text{SRM987}}$ systematics across multiple carbonate reference materials remain scarce. Given the expanding use of stable Sr isotopes in reconstructing marine carbonate system dynamics,^{7,8} establishing an optimized pretreatment procedure is essential. Accordingly, this study examines the effects of sequential leaching on both radiogenic and stable Sr isotope ratios in carbonate rocks using reference materials. Specifically, we analyzed JLS-1 (limestone), JDO-1 (dolostone), and NIST SRM 1d (argillaceous limestone) to characterize the progressive isotopic changes associated with successive leaching steps.

EXPERIMENTAL

Reference Materials. Three carbonate rock reference materials (Table 1) were selected to evaluate the effects of sequential leaching on Sr isotope compositions. JLs-1 is a dark grey limestone reference material prepared and distributed by the Geological Survey of Japan (GSJ) which was collected from the Garo Mine in Hokkaido, northern Japan. JLs-1 consists primarily of low-Mg calcite (>99%) and contains minor amounts of kaolinite.³⁰ Reported Sr isotope values for JLs-1 include a $R(^{87}\text{Sr}/^{86}\text{Sr})$ of 0.707834 ± 0.000024 (2SD, $n=5$) and a $\delta^{88}\text{Sr}/^{86}\text{Sr}_{\text{SRM987}}$ value of $0.26 \pm 0.03\%$ (2SD, $n=3$).^{26,31–35}

JDo-1 is a grey dolostone reference material also distributed by GSJ and was collected from Kuzuu district, Tochigi Prefecture, central Japan. JDo-1 is characterized by low concentrations of most trace elements and is dominated by Ca and Mg, with carbonate minerals accounting for more than 95% of the bulk composition, and exhibits relatively elevated F and Zn contents typical of the Kuzuu dolomite deposits.^{30,36} Reported Sr isotope values for JDo-1 include a $R(^{87}\text{Sr}/^{86}\text{Sr})$ of 0.707565 ± 0.000066 (2SD, $n=4$) and one $\delta^{88}\text{Sr}/^{86}\text{Sr}_{\text{SRM987}}$ value of $0.25 \pm 0.08\%$.^{18,33,34,37}

The third material, SRM 1d, is an argillaceous limestone distributed by the NIST and represents a relatively recently established carbonate reference material. The material was collected from Putnam County, Indiana, USA. SRM 1d consists predominantly of carbonate minerals (>90%), with a substantial clay mineral component reflected by elevated Al and Si concentrations relative to pure limestones.³⁸ Published Sr isotope data for SRM 1d remain limited compared to other carbonate standards, with reported values of 0.708080 ± 0.000016 for $R(^{87}\text{Sr}/^{86}\text{Sr})$ and $0.35 \pm 0.03\%$ for $\delta^{88}\text{Sr}/^{86}\text{Sr}_{\text{SRM987}}$.³⁸ Owing to its relatively high clay content, a previous study has noted that the Sr isotopic composition of SRM 1d may vary depending on the leaching method applied.³⁸ Together, these three reference materials encompass a representative range of carbonate mineralogies and impurity contents, enabling a systematic assessment of leaching behavior and Sr isotope fractionation across diverse carbonate matrices.

Sample digestion and column chemistry. All experiments were conducted at the Korea Institute of Geoscience and Mineral Resources (KIGAM), South Korea. Ultrapure nitric acid (HNO_3) and hydrochloric acid (HCl), glacial acetic acid ($\geq 99.99\%$), and ammonium acetate ($\geq 99.99\%$) were obtained from Merck (Darmstadt, Germany). Deionized water was produced using a Milli-Q system (Millipore, Milford, USA) and used throughout the study.

The sequential leaching procedure employed in this study was based on the method described by Bellefroid *et al.* (Table 2).¹⁵

Table 1. Bulk-leach $R_{\text{con}}(^{87}\text{Sr}/^{86}\text{Sr})$ and $\delta^{88}\text{Sr}/^{86}\text{Sr}_{\text{SRM987}}$ values of carbonate rock reference materials with published data

Reference material	$R_{\text{con}}(^{87}\text{Sr}/^{86}\text{Sr}) (\pm 2\text{SD})$	$\delta^{88}\text{Sr}/^{86}\text{Sr}_{\text{SRM987}} (\%) (\pm 2\text{SD})$	Ref.
JLs-1	0.70784 ± 0.000025 ($n=14$)		34
	0.70785 ± 0.00003 ($n=3$)	0.26 ± 0.04 ($n=3$)	33
	0.70782 ± 0.00000 ($n=2$)	0.241 ± 0.034 ($n=8$)	26
	0.707825 ± 0.000014 ($n=3$)		35
		0.273 ± 0.056 ($n=8$)	39
	0.707833 ± 0.000029 ($n=4$)		31
	0.707865 ± 0.000031 ($n=4$)	0.253 ± 0.029 ($n=4$)	This study
JDo-1	0.70760 ± 0.000156 ($n=22$)		34
	0.707565 ± 0.000020 ($n=8$)		37
	0.70752 ± 0.00001 ($n=3$)	0.25 ± 0.08 ($n=3$)	33
	0.707566 ± 0.000016 ($n=3$)		18
	0.707560 ± 0.000037 ($n=2$)	0.247 ± 0.030 ($n=2$)	This study
SRM 1d	0.708080 ± 0.000016 ($n=11$)	0.35 ± 0.03 ($n=11$)	38
	0.708200 ± 0.000004 ($n=2$)	0.315 ± 0.017 ($n=2$)	This study

Table 2. Sequential leaching protocol

Steps	Reagents	Protocol
	200 mg of powdered rock samples to 15 ml centrifuge tube	
P1-P2	2 x 7 ml of 1 mol/L ammonium acetate	Ultrasonic bath (30 min) and centrifugation
Washing	Rinse with deionized water	(3000 rpm for 5 min) for each step
L1-L4	4 x 10 ml of 0.05 mol/L acetic acid	
L5-L6	2 x 10 ml of 0.2 mol/L acetic acid	
L7	10 ml of 1 mol/L acetic acid	

Approximately 200 mg of powdered rock samples were weighed into 15 mL centrifuge tubes. The samples were first treated twice with 7 mL of 1 mol/L ammonium acetate (P1-P2). After a rinse with deionized water, the residue was leached four times with 10 mL of 0.05 mol/L acetic acid (L1-L4), followed by two leaches with 0.2 mol/L acetic acid (L5-L6) and a final leach with 1 mol/L acetic acid (L7). The leaching procedure was designed to ensure sufficient dissolution to capture progressive changes in the leachate composition, approaching near-complete dissolution of the sample. After the final leaching step (L7), little to no visible residue remained for JLs-1 and JDo-1, and only minor residual particles were observed in SRM 1d. For each leaching step, samples were reacted for 30 min in an ultrasonic bath at room temperature, followed by centrifugation at 3000 rpm for 5 min. The supernatant was collected, and the remaining residue was subjected to the subsequent leaching step. All collected supernatants were filtered through 0.22 μm syringe filters, evaporated to dryness at 80°C on a hot plate, and redissolved in 1.5 mL of 8 mol/L HNO_3 for column chemistry. For the analysis of bulk carbonate reference materials, approximately 200 mg of powdered samples were dissolved in 10 mL of aqua regia for 24 hours. Following dissolution, no significant solid residue remained, except for minor insoluble particles. The solutions were evaporated to dryness at 80°C on a hot plate, redissolved in 2% HNO_3 , filtered through 0.22 μm syringe filters, and stored prior to analysis.

Strontium purification was performed using 2 mL Sr-Spec resin cartridges (Eichrom Technologies, USA) operated with a vacuum box system (Table 3).³⁹ Prior to sample loading, the columns were thoroughly cleaned to minimize blank levels and memory effects by washing with 50 mL of 8 mol/L HNO₃ followed by 60 mL of 0.05 mol/L HNO₃. The columns were then conditioned with 10 mL of 8 mol/L HNO₃. Samples, containing approximately 1 μg of Sr dissolved in 1.5 mL of 8 mol/L HNO₃, were loaded onto the conditioned columns. Matrix elements were removed by rinsing with 11.5 mL of 8 mol/L HNO₃, and Sr was subsequently eluted with 50 mL of 0.05 mol/L HNO₃. The collected Sr eluates were evaporated to dryness at 80°C on a hotplate, treated with concentrated HNO₃, dried again, and finally redissolved in 2% HNO₃ for elemental and isotopic analysis (Table S1). During all column processes, the tail of the elution body and blanks were collected, and the Sr recovery rate for all samples is 99±3% (2SD). Procedural blanks were monitored regularly and were insignificant, accounting for less than 0.1% of the ⁸⁸Sr signal intensity of the samples. To evaluate procedural reproducibility, JLs-1 was processed in duplicate beginning from the dissolution step (Fig. S1, Table S2). Two independently dissolved aliquots of JLs-1 were processed separately through the entire column purification and analytical procedure. The two independent sequential leaching experiments yielded $R(^{87}\text{Sr}/^{86}\text{Sr})$ and $\delta^{88}\text{Sr}/^{86}\text{Sr}_{\text{SRM987}}$ values that were in close agreement, with minor differences that slightly exceed analytical uncertainty but do not affect the interpretation of the results.

Instrumental analysis. The element concentrations of the sequential leaching samples were analyzed using ICP-MS (PerkinElmer NexION 350) and ICP-OES (PerkinElmer Optima 5300), and Sr isotopic ratios were measured using MC-ICP-MS (Neptune Plus, Thermo Fisher Scientific) with wet plasma setting, all conducted at the KIGAM. The faraday cup configuration of MC-ICP-MS was arranged to simultaneously monitor signal intensities for ⁸³Kr, ⁸⁵Rb, ⁸⁶Sr, ⁸⁷Sr, ⁸⁸Sr, ⁹⁰Zr, and ⁹²Zr. Specifically, ⁸³Kr and ⁸⁵Rb were monitored to correct for the isobaric interferences of ⁸⁶Kr on ⁸⁶Sr and ⁸⁷Rb on ⁸⁷Sr, respectively ($R(^{83}\text{Kr}/^{86}\text{Kr}) = 0.664740$; $R(^{87}\text{Rb}/^{85}\text{Rb}) = 0.385617$; IUPAC data³⁷). An exponential equation was used to estimate isobaric interferences, which were then corrected by subtracting the calculated contributions.^{41,42} A summary of the primary instrument operating parameters is provided in Table 4.

Instrumental mass bias was corrected using Zr-doped standard-sample bracketing technique (Zr-doped SSB), as the SSB method alone cannot fully correct for temporal mass bias drift during a measurement sequence.^{33,41,43,44} NIST SRM 987 was used as the bracketing standard, and NIST SRM 3169 was employed for Zr doping. Prior to analysis, all sample and bracketing solutions were doped with a Zr standard material, with Sr and Zr concentrations adjusted to 200 ppb (2.28 μmol/L) and 400 ppb (4.38 μmol/L), respectively, to ensure comparable intensities of ⁸⁸Sr and ⁹⁰Zr. The

Table 3. Strontium purification procedure

Step	Reagent	Volume (mL)
Pre-cleaning	8 mol/L HNO ₃	50
	Deionized water	10
	0.05 mol/L HNO ₃	60
Conditioning	8 mol/L HNO ₃	10
Sample loading	8 mol/L HNO ₃	1.5
Removal of matrix	8 mol/L HNO ₃	11.5
Collection of Sr	0.05 mol/L HNO ₃	50

Table 4. Instrumental and operating parameters of MC-ICP-MS

Variables	Setting
RF power	1200 W
Plasma condition	Wet
Sample gas flow rate	~1.0 L/min
Auxiliary gas flow rate	1 L/min
Sample cone	Nickel, 1.1 mm orifice
Skimmer cone	Nickel, 0.8 mm orifice
Sample uptake	80-100 μL/min
Wash time	300 s
Lens and Zoom optics	Optimized for maximum signal intensity and stability in each session
Measurement mode	Static
Cup configuration	L4: ⁸³ Kr, L3: ⁸⁴ Sr, L2: ⁸⁵ Rb, L1: ⁸⁶ Sr, Ax: ⁸⁷ Sr, H1: ⁸⁸ Sr, H2: ⁹⁰ Zr, H3: ⁹¹ Zr, H4: ⁹² Zr
Sensitivity	200 ppb of Sr: 15 V on ⁸⁸ Sr ion-beam
Analysis concentration	Sr: 200 ppb / Zr: 400 ppb
Integration time (s)	4.194
Acquisition protocol	1 block 50 cycles

average ⁸⁸Sr/⁹⁰Zr beam intensity ratio was 1.02±0.09 (2SD, n=67). The corrected Sr stable isotope ratio $\left(\frac{^{88}\text{Sr}}{^{86}\text{Sr}}\right)_{\text{corr}}$ was derived from the measured $R(^{92}\text{Zr}/^{90}\text{Zr})$ using the exponential law:

$$\left(\frac{^{88}\text{Sr}}{^{86}\text{Sr}}\right)_{\text{corr}} = \left(\frac{^{88}\text{Sr}}{^{86}\text{Sr}}\right)_{\text{meas}} \times \left[\frac{R(^{92}\text{Zr}/^{90}\text{Zr})_{\text{true}}}{R(^{92}\text{Zr}/^{90}\text{Zr})_{\text{meas}}} \right]^{\left[\ln \frac{M_{88}}{M_{86}} / \ln \frac{M_{92}}{M_{90}} \right]} \quad (2)$$

where $\left(\frac{^{88}\text{Sr}}{^{86}\text{Sr}}\right)_{\text{meas}}$ is the analyzed ratio after correction for Kr and Rb isobaric interferences, $\left(\frac{^{92}\text{Zr}}{^{90}\text{Zr}}\right)_{\text{meas}}$ is the measured Zr isotope ratio, $\left(\frac{^{92}\text{Zr}}{^{90}\text{Zr}}\right)_{\text{true}}$ is the reference isotopic ratio of 0.333333 (IUPAC data³⁷). M denotes the absolute mass of each isotope. The $R(^{92}\text{Zr}/^{90}\text{Zr})$ was selected as the primary parameter for normalization because its mass difference (2 amu) matches that of the target $R(^{88}\text{Sr}/^{86}\text{Sr})$, thereby better capturing mass-dependent instrumental fractionation than the method using $R(^{91}\text{Zr}/^{90}\text{Zr})$.^{42,45} For comparison with conventional radiogenic values, $R(^{87}\text{Sr}/^{86}\text{Sr})$ was corrected by internal normalization with $R(^{88}\text{Sr}/^{86}\text{Sr}) = 8.375209$ (IUPAC data⁴⁰) and is hereafter referred to $R_{\text{con}}(^{87}\text{Sr}/^{86}\text{Sr})$. Stable Sr isotope compositions are reported in the standard delta notation relative to the isotopic reference material NIST SRM 987. Repeated analysis of SRM 987 solutions yielded $R_{\text{con}}(^{87}\text{Sr}/^{86}\text{Sr}) = 0.710291 \pm 0.000028$ (2SD, n=67) and $\delta^{88}\text{Sr}/^{86}\text{Sr}_{\text{SRM987}} = -0.002 \pm 0.035$ (2SD, n=37).

RESULTS AND DISCUSSION

Bulk isotopic compositions and matrix effect. Molar element ratios, $R_{\text{con}}(^{87}\text{Sr}/^{86}\text{Sr})$, and $\delta^{88}\text{Sr}/^{86}\text{Sr}_{\text{SRM987}}$ values for each sequential leaching step are shown in Table S1. The cumulative recovery of major elements ranges from 92 to 104% of the recommended bulk values, with one exception, indicating generally good mass balance (see Table S1 and the accompanying note for details). The bulk Sr isotopic compositions of JLs-1 and JDo-1 obtained in this study are in close agreement with previously published values within analytical uncertainty (Table 1), despite differences in dissolution protocols. In this study, bulk dissolution was performed using aqua regia, whereas earlier studies employed a range of acids, including 1–4 mol/L HCl and HNO_3 .^{18,26,31–35,37} The consistency of bulk Sr isotope values for JLs-1 and JDo-1 across these studies suggests that both materials undergo effective, near-complete dissolution under moderately strong acid conditions, resulting in bulk Sr isotope compositions that are insensitive to acid type or concentration. In contrast, SRM 1d exhibits a more pronounced deviation from previously reported bulk Sr isotope values. The absolute difference between the two mean values is 0.000120, which is ~ 2.8 times larger than the combined uncertainty (≈ 0.000043), indicating the two values are statistically distinguishable. Published data for SRM 1d were obtained using dissolution in 1 mol/L HCl, and the leachate was subsequently separated from the residual solid by centrifugation. Such a procedure represents partial dissolution rather than complete digestion.³⁸ By comparison, the aqua regia digestion applied in this study is expected to dissolve a larger fraction of the sample. Although published data for SRM 1d are limited, the observed offset likely reflects its higher clay mineral content, which makes bulk Sr isotope compositions more sensitive to differences in dissolution procedures.³⁸ This observation further suggests that variations in dissolution procedures may influence the resulting isotopic compositions, particularly for clay-rich carbonate materials. A more detailed discussion of how different dissolution steps affect Sr isotopic compositions is provided in the following section.

In carbonate rocks, where major elements such as Ca are more abundant than Sr, a measurable amount of Ca can remain even after column purification.^{37,46–48} Such residual matrix elements can generate polyatomic interferences on Sr isotopes ($^{44}\text{Ca}^{40}\text{Ar}$, $^{46}\text{Ca}^{40}\text{Ar}$, $^{43}\text{Ca}^{44}\text{Ca}$, $^{44}\text{Ca}^{44}\text{Ca}$) and can alter ion transmission or ionization efficiency relative to standards. Consequently, differences in matrix composition between samples and bracketing standards may lead to differential instrumental mass bias and inaccurate mass bias corrections.^{37,46} Previous studies using wet plasma have reported that Ca/Sr mass ratios as high as ~ 10 in solution do not significantly affect Sr isotope measurements.^{46,48,49} However, Wang *et al.* (2023) using dry plasma demonstrated that even Ca/Sr mass ratios as low as 0.5 can exert a substantial influence on stable Sr isotopic compositions.⁸

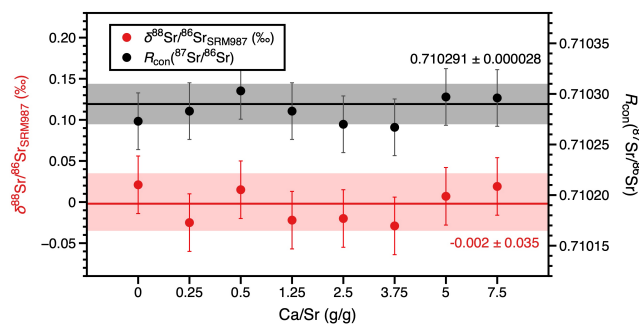


Fig. 1 $R_{\text{con}}(^{87}\text{Sr}/^{86}\text{Sr})$ and $\delta^{88}\text{Sr}/^{86}\text{Sr}_{\text{SRM987}}$ results of 200 ppb SRM 987 solutions mixed with varying amounts of Ca. The black and red lines represent the long-term mean $R_{\text{con}}(^{87}\text{Sr}/^{86}\text{Sr})$ and $\delta^{88}\text{Sr}/^{86}\text{Sr}_{\text{SRM987}}$ values, respectively, and the colored bands denote the corresponding long-term analytical precision (2SD).

This discrepancy likely reflects the higher tolerance of wet plasma to matrix effects relative to dry plasma, consistent with observations from other isotope systems such as Li and Mg.⁴⁷

To assess whether incomplete Ca removal during column purification could bias Sr isotope analysis under our instrumental conditions, a Ca-doping test was performed using the Sr isotope standard NIST SRM 987 and the ICP Ca calibration standard under wet plasma settings. All test solutions were prepared to contain 200 ppb Sr and 400 ppb Zr, with the Ca/Sr mass ratio systematically varied from 0 to 7.5 to evaluate potential matrix effects. The results showed that both $\delta^{88}\text{Sr}/^{86}\text{Sr}_{\text{SRM987}}$ and $R_{\text{con}}(^{87}\text{Sr}/^{86}\text{Sr})$ values remained constant within analytical uncertainty across the entire Ca/Sr range tested, indicating that neither stable nor radiogenic Sr isotope measurements were measurably affected by elevated Ca levels (Fig. 1). These results demonstrate that modest amounts of residual Ca remaining after column purification do not compromise Sr isotope measurements under wet plasma conditions, consistent with previous studies.^{47,48,49} The Ca/Sr mass ratios of all samples after column purification were within this acceptable range, indicating that residual Ca did not introduce measurable matrix effects under our analytical conditions. However, matrix effects may differ under dry plasma conditions⁸, and therefore stricter control of Ca removal during column purification may be required in such analytical setups.

Isotopic composition trends during the pre-leach stage. The sequential leaching procedure begins with the ammonium acetate pre-leaching steps (Table 2, P1-P2). During this stage, all three standards exhibited notably low Ca+Mg content (defined as the combined amount of Ca and Mg released at each leaching step, expressed as a percentage of the total recovered from all steps), indicating that the dissolved fraction was dominated by non-carbonate components rather than by primary carbonate minerals (Fig. 2A). This observation is consistent with previous studies

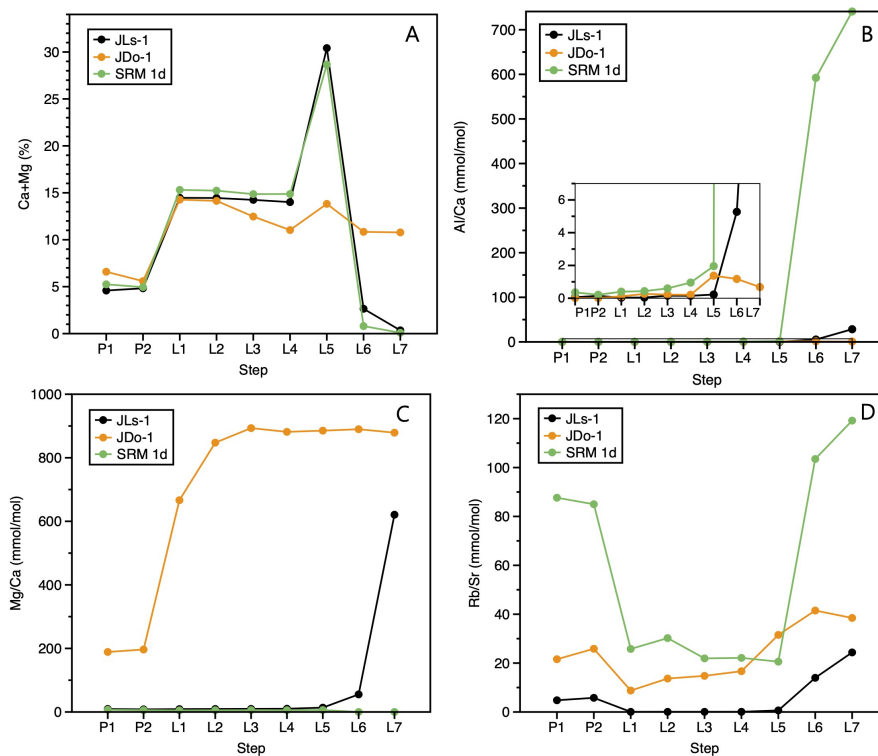


Fig. 2 Leaching patterns for the three carbonate rock reference materials (JLs-1, JDo-1, and SRM 1d). (A) Ca+Mg content, (B) Al/Ca, (C) Mg/Ca, and (D) Rb/Sr ratios. Details for each leaching step are described in the main text.

showing that ammonium acetate pre-leach primarily extracts Sr from exchangeable and surface-adsorbed sites.^{14,15,18,19}

The use of Al and Rb is central to assessing silicate Sr contamination during leaching, yet their sensitivities differ markedly. Because Al is confined to insoluble aluminosilicate phases, elevated Al concentrations in leachates generally reflect the actual dissolution of these minerals and the consequent introduction of detrital source Sr.^{15,50} However, numerous studies have demonstrated that clay-bound Sr can be released through ion-exchange processes during the earliest stages of leaching without measurable dissolution of the aluminosilicate framework.^{14,15,19,20} This means that Al is not a sensitive tracer for the early-stage release of Sr hosted on clay. In contrast, Rb provides a far more responsive indicator because it tracks both exchangeable Sr released from clay mineral interlayer sites and the contribution from detrital or authigenic clay dissolution. Consistent with this pattern, our results show little or no variations in Al/Ca ratios in the initial fractions, whereas Rb/Sr ratios are elevated during these early steps, reflecting the mobilization of exchangeable Sr (Fig. 2B and D).

Numerous studies have documented a strong positive correlation between Rb/Sr (or Rb/Ca) ratios and $R_{\text{con}}(^{87}\text{Sr}/^{86}\text{Sr})$, indicating that inputs from Rb-rich phases, commonly associated with clay minerals, are closely linked to elevated radiogenic Sr

isotope signatures.^{15,18–20} Accordingly, the release of interlayer-bound, clay-associated Sr during the pre-leach stage is accompanied by increased $R_{\text{con}}(^{87}\text{Sr}/^{86}\text{Sr})$ (Figs. 2D, 3A). SRM 1d exhibits a high $R_{\text{con}}(^{87}\text{Sr}/^{86}\text{Sr})$ during the pre-leach stage, along with large variations in Rb/Sr. This result reflects the high clay mineral content of the argillaceous limestone SRM 1d.^{15,20} The slightly lower $\delta^{88}\text{Sr}/^{86}\text{Sr}_{\text{SRM987}}$ values observed in the early leaching fractions suggest that Sr released from clay interlayer sites may have slightly lower $\delta^{88}\text{Sr}/^{86}\text{Sr}_{\text{SRM987}}$ values. However, the magnitude of this difference (0.03–0.05‰) is too small to exert a significant influence on the bulk isotopic composition (Table S1).

In contrast, JLs-1 exhibited relatively stable $R_{\text{con}}(^{87}\text{Sr}/^{86}\text{Sr})$ and Rb/Sr ratios throughout the pre-leach stage, suggesting minimal clay contribution (Figs. 2D, 3A). However, a distinct low $\delta^{88}\text{Sr}/^{86}\text{Sr}_{\text{SRM987}}$ value observed in the first leaching step (P1, Fig. 3B) likely reflects the dissolution of isotopically light Sr from surface-adsorbed phases. Although comparable sequential leaching step-specific datasets are scarce for stable Sr isotopes, analogous characteristic has been reported for other divalent metals in carbonates. For example, Lin *et al.* (2020) showed that soluble and exchangeable Ba fractions extracted from JLs-1 exhibit lower $\delta^{137}\text{Ba}/^{134}\text{Ba}$ values than the carbonate mineral fraction, which they attributed to surface-adsorption effects during early diagenesis.⁵¹ Similarly, adsorbed Sr is inferred to be isotopically

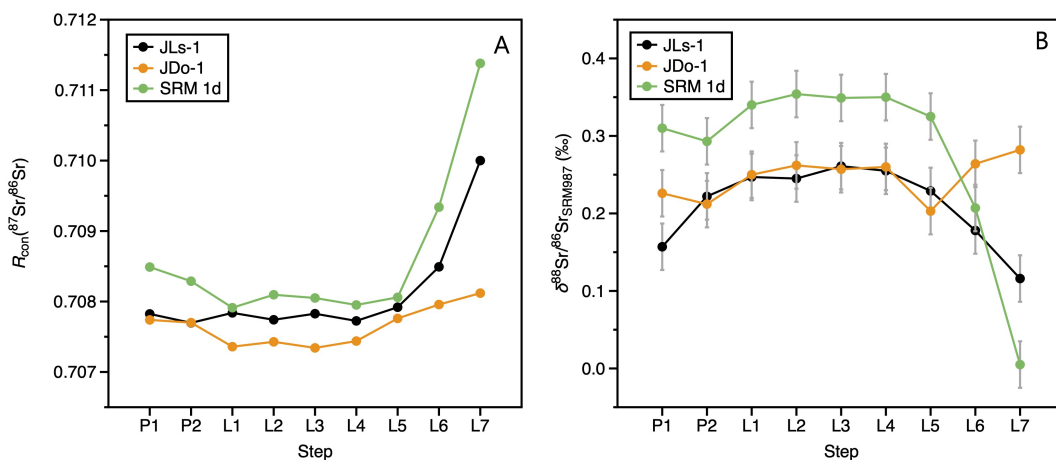


Fig. 3 Changes in (A) $R_{\text{con}}(^{87}\text{Sr}/^{86}\text{Sr})$ and (B) $\delta^{88}\text{Sr}/^{86}\text{Sr}_{\text{SRM987}}$ for three reference materials across the sequential leaching steps. Error bars for $R_{\text{con}}(^{87}\text{Sr}/^{86}\text{Sr})$ are smaller than the symbol size. Details for each leaching step are described in the main text.

lighter; however, its limited abundance restricts this isotopic signal to the first pre-leach fraction.

For JDo-1, the pre-leach steps exhibited slightly higher values in $R_{\text{con}}(^{87}\text{Sr}/^{86}\text{Sr})$ relative to the subsequent leaching steps (Fig. 3A). This trend can be attributed to the preferential dissolution of the small amount of calcite present in JDo-1 (<1%) over dolomite, as calcite is more soluble and releases Sr earlier during the leaching process.¹⁸ The Mg/Ca ratios of the leachates further support this interpretation. While the bulk JDo-1 has an Mg/Ca ratio of approximately 755 mmol/mol³⁰, the initial leachates (P1-P2) display significantly lower values (Fig. 2C, ~200 mmol/mol), indicating that the dissolved phase was predominantly calcite rather than dolomite.^{17,18,20} Concurrently, the slightly elevated Rb/Sr ratios in this interval suggest a minor contribution from clay minerals, which likely accounts for the moderately lower $\delta^{88}\text{Sr}/^{86}\text{Sr}_{\text{SRM987}}$ values (0.03-0.04‰) observed in the early fractions, similar to the trend in SRM 1d (Fig. 2D, 3B). However, as observed in SRM 1d, this deviation is not statistically significant when considering analytical uncertainty, suggesting that the contribution of these early-stage components to the bulk isotopic composition is negligible.

These results demonstrate that the ammonium acetate pre-leaching step is effective in minimizing the contribution of non-carbonate minerals, thereby preserving the primary Sr isotopic signal. In samples containing clay minerals, this procedure successfully removes exchangeable Sr from interlayer sites, a process more reliably traced by Rb/Sr ratios than Al/Ca ratios. Furthermore, the dissolution of easily soluble surface-adsorbed phases during pre-leaching further reduces the risk of contamination from secondary calcites. Pre-leaching is particularly critical for dolostone samples to isolate the pure

dolomite signal by preferentially dissolving trace amounts of calcite. Radiogenic Sr isotope ratios in the pre-leach fractions differ from subsequent leachates by up to 0.0004-0.0005, indicating a potentially significant influence on analytical results if not removed. Although $\delta^{88}\text{Sr}/^{86}\text{Sr}_{\text{SRM987}}$ is generally less susceptible to contributions from early leaching steps than $R_{\text{con}}(^{87}\text{Sr}/^{86}\text{Sr})$, samples subjected to diagenesis or containing abundant clay minerals can exhibit significant isotopic deviations, underscoring the importance of careful pretreatment.

Evolution of Sr isotopes during the later leaching stage. In the later stages of the leaching sequence (L5-L7), corresponding to the higher concentration acetic acid steps (Table 2), JLS-1 and SRM 1d exhibited pronounced increases in Al/Ca and Rb/Sr ratios, suggesting the dissolution of clay minerals (Fig. 2B and D).^{15,19,52} Consistent with previous studies documenting elevated $^{87}\text{Sr}/^{86}\text{Sr}$ signals associated with clay mineral dissolution,^{14,18,20} the $R_{\text{con}}(^{87}\text{Sr}/^{86}\text{Sr})$ values of both samples increased as leaching proceeded (Fig. 3A). JLS-1 showed differences of up to ~0.002 between the early acetic acid fractions (L1-L4) and late leaching steps (L5-L7), whereas SRM 1d exhibited even larger shifts of up to ~0.003 (Fig. 3A). These differences are significantly larger than the analytical uncertainty, indicating that the observed shifts are statistically meaningful. The greater magnitude of change in SRM 1d reflects its higher clay mineral content, underscoring the importance of clay abundance in the sample during the pretreatment process. A comparable trend was found for $\delta^{88}\text{Sr}/^{86}\text{Sr}_{\text{SRM987}}$. Dissolution of clay minerals resulted in decreases of up to ~0.15‰ for JLS-1 and up to ~0.35‰ for SRM 1d (Fig. 3B). Although soil $\delta^{88}\text{Sr}/^{86}\text{Sr}_{\text{SRM987}}$ values span a broad range (0.02-0.37‰)⁵⁰, clays typically exhibit lower $\delta^{88}\text{Sr}/^{86}\text{Sr}_{\text{SRM987}}$ because secondary mineral formation during weathering preferentially incorporates isotopically light ^{86}Sr into the solid phase.^{54,55} Hence,

the lower $\delta^{88}\text{Sr}/^{86}\text{Sr}_{\text{SRM987}}$ values observed in the late-stage leachates of JLs-1 and SRM 1d can be attributed to the dissolution of isotopically light clay minerals.

JDo-1 displays a distinct leaching behavior compared with the other two standards. The minimal variations in Al/Ca ratios correspond to the smallest changes observed in $R_{\text{con}}(^{87}\text{Sr}/^{86}\text{Sr})$ values, suggesting that the contribution from clay minerals is relatively limited (Figs. 2B, 3A). Although the exact clay mineral abundances of the three standards are not available for direct comparison, the muted radiogenic Sr response implies that JDo-1 contains less clay than JLs-1 and SRM 1d. Despite this, a notable feature of JDo-1 is that clay mineral dissolution appears to initiate earlier. An increase in Al/Ca is first observed at L5, where acetic acid concentration becomes high (Fig. 2B). The steepest rise in $R_{\text{con}}(^{87}\text{Sr}/^{86}\text{Sr})$ values also occurs between L4 and L5, and Rb/Sr increases sharply at the same step, indicating the onset of significant clay dissolution beginning in L5. This dissolution likely accounts for the lower $\delta^{88}\text{Sr}/^{86}\text{Sr}_{\text{SRM987}}$ observed in L5.

Unlike JLs-1 and SRM 1d, however, the isotopic effects of clay dissolution in JDo-1 do not intensify toward the later steps. This difference can be explained by the persistent dissolution of dolomite, which constitutes the dominant mineral phase in JDo-1. Dolomite continues to dissolve throughout the later stages of the experiment, as evidenced by the nearly constant Ca+Mg contents and Mg/Ca ratios from L5 to L7 (Fig. 2A and C). Consequently, the leachates in the late steps are not dominated by clay-derived components but instead reflect a mixture in which dolomite dissolution remains substantial. This continuous input of dolomite-derived Sr likely buffers the isotopic composition and suppresses the extent of clay-driven shifts, resulting in smaller isotopic deviations in the later fractions compared with JLs-1 and SRM 1d.

Taken together, the later stages of the leaching experiments demonstrate that the extent and timing of clay mineral dissolution exert a primary control on both radiogenic and stable Sr isotope variations in the leachates. JLs-1 and SRM 1d show progressive and substantial isotopic shifts associated with the clay dissolution, whereas JDo-1 exhibits a more subdued response due to its lower clay content and the buffering effect of continuous dolomite dissolution. These contrasting behaviors illustrate that the mineralogical composition of a sample strongly influences the evolution of Sr isotopes during leaching. Consequently, careful selection of pretreatment strategies is essential when analyzing carbonate sample with varied mineralogies.

Implications for marine Sr isotope reconstruction. The combined isotopic and elemental data reveal that both early and late leaching steps are affected by non-carbonate Sr reservoirs. During the pre-leaching step, approximately 10-20% of the total Sr is released, primarily corresponding to surface-adsorbed and ion-exchangeable Sr. After the initial pre-leaching steps, both

isotope ratios and clay-sensitive elemental ratios (e.g., Al/Ca, Rb/Sr) remain relatively stable across the middle fractions (L1-L4), indicating dominance of carbonate dissolution. At later stages, these parameters begin to shift, reflecting increasing contributions from non-carbonate components. The transition between these trends occurs when approximately 50-60% of the total Sr (or Ca) has been released, providing a practical basis for defining the carbonate-dominated dissolution interval for these reference materials. Accordingly, to obtain Sr isotope compositions minimally affected by non-carbonate contributions in these reference materials, we recommend removing the initial ~10-20% of total Sr released during pre-leach with 1 mol/L ammonium acetate and restricting subsequent dissolution using 0.05 mol/L acetic acid to the next 50-60% of total Sr (or Ca) released. Applying this procedure, the mean values of the middle fractions (L1-L4) yield representative Sr isotope compositions for primary marine carbonates, with recommended $R_{\text{con}}(^{87}\text{Sr}/^{86}\text{Sr})$ values of 0.707783 ± 0.000028 for JLs-1, 0.707386 ± 0.000028 for JDo-1, and 0.708008 ± 0.000028 for SRM 1d, and corresponding $\delta^{88}\text{Sr}/^{86}\text{Sr}_{\text{SRM987}}$ values of $0.252 \pm 0.035\%$, $0.256 \pm 0.035\%$, and $0.325 \pm 0.035\%$, respectively (Table S3). Reported uncertainties are based on the reproducibility of repeated analysis of the bracketing standard material.

A comparison between the recommended Sr isotope ratios and the values obtained using the entire set of leachates (P1-L7), calculated as a Sr-weighted average of all fractions, shows that the differences in $R_{\text{con}}(^{87}\text{Sr}/^{86}\text{Sr})$ values exceed analytical precision (Fig. 4A). Although the offsets in stable Sr isotopes are relatively small, $\delta^{88}\text{Sr}/^{86}\text{Sr}_{\text{SRM987}}$ values tend to be higher when calculated using only the middle fractions, consistent with previous observations that weaker acid used in bulk leaching of JLs-1 yield higher $\delta^{88}\text{Sr}/^{86}\text{Sr}_{\text{SRM987}}$ values than strong acid.²⁶ The largest discrepancy in $\delta^{88}\text{Sr}/^{86}\text{Sr}_{\text{SRM987}}$ occurs in SRM 1d, the sample that contains the highest clay mineral content (Fig. 4B). Although SRM 1d is an argillaceous limestone, it still consists of more than 90% carbonate. In natural samples, however, carbonate contents can be substantially lower, often as little as 50-60%.⁵⁶⁻⁵⁸ As a result, the isotopic offsets are likely to be even larger in typical geological samples.

Because this study focuses on carbonate reference materials, the recommended pretreatment procedure should be regarded as an empirical guideline rather than a universally applicable threshold. The position and extent of the carbonate-dominated dissolution interval may vary depending on mineralogy, clay abundance, and texture in natural carbonate samples. Previous studies have proposed a wide range of leaching strategies depending on sample characteristics. The proportion removed during pre-leaching varies from as little as ~5% to as much as 30-40%, while the fraction selected for analysis ranges from subsequent 10% to 40% of the total Sr released.^{13,18,20} Bellefroid *et al.* (2018) further demonstrated that the carbonate-dominated fraction can vary even

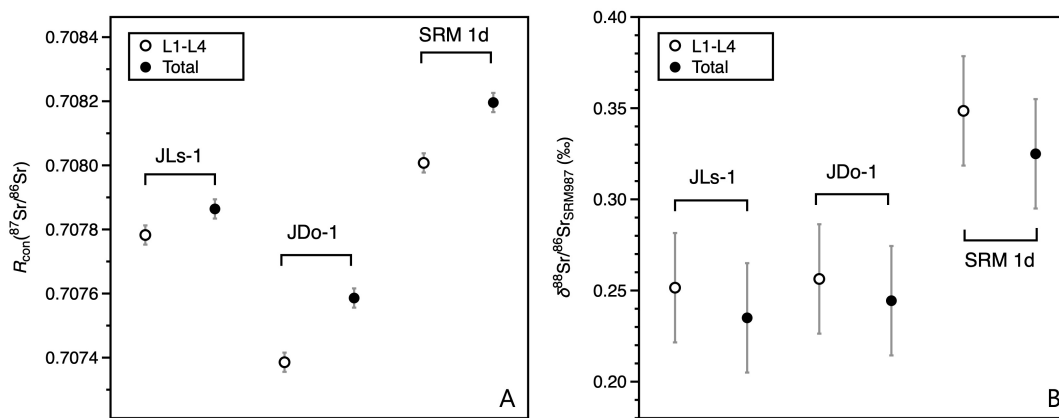


Fig. 4 Differences in (A) $R_{\text{con}}(^{87}\text{Sr}/^{86}\text{Sr})$ and (B) $\delta^{88}\text{Sr}/^{86}\text{Sr}_{\text{SRM987}}$ values obtained using two leaching approaches. Open symbols represent isotopic compositions calculated using only the intermediate fractions (excluding the pre-leach steps, P1-P2, and the later steps, L5-L7), whereas filled symbols represent values calculated using all leaching steps.

within samples from the same geological formation.¹⁵ These variations highlight that fixed percentage-based approaches may not be universally applicable. Therefore, for natural carbonate samples, it is necessary to identify an appropriate leaching interval that best preserves the primary carbonate signal by selecting representative samples that reflect the local mineralogy and clay mineral abundance.

In a broader paleo-environmental context, these results demonstrate that careful selection of leaching fractions is essential for recovering uncontaminated marine Sr signals. Adoption of the proposed pretreatment strategy enhances the precision and comparability of carbonate-based Sr isotope datasets, thereby improving the reliability of seawater Sr isotope reconstructions throughout geologic time.

CONCLUSION

This study provides $\delta^{88}\text{Sr}/^{86}\text{Sr}_{\text{SRM987}}$ and $R_{\text{con}}(^{87}\text{Sr}/^{86}\text{Sr})$ values for three widely used carbonate standards—particularly NIST SRM 1d, for which few data have previously been available—thereby improving the characterization of reference materials for Sr isotope research. We systematically evaluated the effects of sequential leaching on radiogenic and stable Sr isotopes to establish an optimized pretreatment strategy for isolating primary carbonate Sr signals in carbonate reference materials. Early and late leaching steps were strongly influenced by non-carbonate Sr reservoirs, whereas only the intermediate fractions reflected dissolution of primary calcite or dolomite and yielded isotopic values representative of the original marine signal. Because this study focuses on carbonate reference materials, the application of the pretreatment procedure to natural samples requires careful

consideration, as the position and extent of the carbonate-dominated dissolution interval may vary depending on mineralogy, clay abundance, and texture. Overall, the proposed framework enhances analytical accuracy and provides a foundation for future studies linking Sr isotopes to marine chemical evolution, particularly when combined with careful assessment of leaching behavior in complex natural carbonate systems.

ASSOCIATED CONTENT

The supporting information (Tables S1-S3 and Fig. S1) is available at <https://www.at-spectrosc.com>.

AUTHOR INFORMATION



Jena Jeong received her M.S. degree in 2023 and is currently a PhD student in geochemistry at Seoul National University and a research student at the Korea Institute of Geoscience and Mineral Resources. Her research focuses on stable isotope geochemistry of carbonate rocks to investigate weathering processes and climate evolution. She specializes in high-

precision MC-ICP-MS analysis and aims to reconstruct marine geochemical cycles and paleoenvironmental conditions through accurate measurements of multiple stable isotope systems.



Youngsook Huh received her PhD in marine chemistry and geochemistry from the Massachusetts Institute of Technology in 1998. She is currently a professor in the School of Earth and Environmental Sciences at Seoul National University. Her research focuses on isotope and trace element geochemistry applied to Earth-surface and paleoenvironmental processes, with

particular emphasis on geochemical fluxes linking continental and marine systems over geological timescales.

Corresponding Author

* J. Jeong

Email address: jena.jeong13@gmail.com

* Y. Huh

Email address: yhuh@snu.ac.kr

Notes

The authors declare no competing financial interest.

ACKNOWLEDGMENTS

This research was supported by the National Research Foundation of Korea (NRF) grants funded by the Korean government (MSIT) (RS-2024-00347048). We would like to thank the four anonymous reviewers for their helpful comments which significantly improved the manuscript.

REFERENCES

1. J. Veizer, D. Ala, K. Azmy, P. Bruckschen, D. Buhl, F. Bruhn, G. A. F. Carden, A. Diener, S. Ebner, Y. Godderis, T. Jasper, C. Korte, F. Pawellek, O. G. Podlaha, and H. Strauss, *Chem. Geol.*, 1999, **161**, 59–88. [https://doi.org/10.1016/S0009-2541\(99\)00081-9](https://doi.org/10.1016/S0009-2541(99)00081-9).
2. C. T. Edwards, M. R. Saltzman, S. A. Leslie, S. M. Bergström, A. R. C. Sedlacek, A. Howard, J. A. Bauer, W. C. Sweet, and S. A. Young, *Geol. Soc. Am. Bull.*, 2015, **127**, 1275–1289. <https://doi.org/10.1130/B31149.1>
3. W. H. Burke, R. E. Denison, E. A. Hetherington, R. B. Koepnick, H. F. Nelson, and J. B. Otto, *Geology*, 1982, **10**, 516–519. [https://doi.org/10.1130/0091-7613\(1982\)10%253C516:VOSSTP%253E2.0.CO;2](https://doi.org/10.1130/0091-7613(1982)10%253C516:VOSSTP%253E2.0.CO;2)
4. D. A. Hodell, G. A. Mead, and P. A. Mueller, *Chem. Geol.*, 1990, **80**, 291–307. [https://doi.org/10.1016/0168-9622\(90\)90011-Z](https://doi.org/10.1016/0168-9622(90)90011-Z)
5. M. R. Palmer and J. M. Edmond, *Earth Planet. Sci. Lett.*, 1989, **92**, 11–26. [https://doi.org/10.1016/0012-821X\(89\)90017-4](https://doi.org/10.1016/0012-821X(89)90017-4)
6. J. M. McArthur, R. J. Howarth, G. A. Shields, and Y. Zhou, *Geologic Time Scale 2020*, 2020, 211–238. <https://doi.org/10.1016/C2020-1-02369-3>
7. A. Paytan, E. M. Griffith, A. Eisenhauer, M. P. Hain, K. Wallmann, and A. Ridgwell, *Science*, 2021, **371**, 1346–1350. <https://doi.org/10.1126/science.aaz9266>
8. J. Wang, L. G. Tarhan, A. D. Jacobson, A. M. Oehlert, and N. J. Planavsky, *Nature*, 2023, **615**, 265–269. <https://doi.org/10.1038/s41586-022-05654-5>
9. A. Krabbenhöft, A. Eisenhauer, F. Böhm, H. Vollstaedt, J. Fietzke, V. Liebetrau, N. Augustin, B. Peucker-Ehrenbrink, M. N. Müller, C. Horn, B. T. Hansen, N. Nolte, and K. Wallmann, *Geochim. Cosmochim. Acta*, 2010, **74**, 4097–4109. <https://doi.org/10.1016/j.gca.2010.04.009>
10. H. Vollstaedt, A. Eisenhauer, K. Wallmann, F. Böhm, J. Fietzke, V. Liebetrau, A. Krabbenhöft, J. Farkaš, A. Tomašových, J. Raddatz, and J. Veizer, *Geochim. Cosmochim. Acta*, 2014, **128**, 249–265. <https://doi.org/10.1016/j.gca.2013.10.006>
11. F. Böhm, A. Eisenhauer, J. Tang, M. Dietzel, A. Krabbenhöft, B. Kisakürek, and C. Horn, *Geochim. Cosmochim. Acta*, 2012, **93**, 300–314. <https://doi.org/10.1016/j.gca.2012.04.038>
12. M. N. Müller, A. Krabbenhöft, H. Vollstaedt, F. P. Brandini, and A. Eisenhauer, *Geobiology*, 2018, **16**, 297–306. <https://doi.org/10.1111/gbi.12276>
13. D. Li, G. A. Shields-Zhou, H.-F. Ling, and M. Thirlwall, *Chem. Geol.*, 2011, **290**, 133–144. <https://doi.org/10.1016/j.chemgeo.2011.09.004>
14. T. R. Bailey, J. M. McArthur, H. Prince, and M. F. Thirlwall, *Chem. Geol.*, 2000, **167**, 313–319. [https://doi.org/10.1016/S0009-2541\(99\)00235-1](https://doi.org/10.1016/S0009-2541(99)00235-1)
15. E. J. Bellefroid, N. J. Planavsky, N. R. Miller, U. Brand, and C. Wang, *Chem. Geol.*, 2018, **497**, 88–99. <https://doi.org/10.1016/j.chemgeo.2018.08.025>
16. G. Bayon, C. R. German, R. M. Boella, J. A. Milton, R. N. Taylor, and R. W. Nesbitt, *Chem. Geol.*, 2002, **187**, 179–199. [https://doi.org/10.1016/S0009-2541\(01\)00416-8](https://doi.org/10.1016/S0009-2541(01)00416-8)
17. K. Zhang, X.-K. Zhu, and B. Yan, *Chem. Geol.*, 2015, **412**, 82–91. <https://doi.org/10.1016/j.chemgeo.2015.07.027>
18. Y. Li, C. Li, and J. Guo, *Microchem. J.*, 2020, **154**, 104607. <https://doi.org/10.1016/j.microc.2020.104607>
19. C. Liu, Z. Wang, and T. D. Raub, *Chem. Geol.*, 2013, **351**, 95–104. <https://doi.org/10.1016/j.chemgeo.2013.05.012>
20. X. Chen and Y. Zhou, *Geostand. Geoanal. Res.*, 2023, **48**, 57–75. <https://doi.org/10.1111/ggr.12531>
21. I. Gorokhov, M. A. Semikhatov, A. V. Baskakov, E. P. Kutyavin, N. N. Melnikov, A. V. Sochava, and T. L. Turchenko, *Stratigr. Geol. Correl.*, 1995, **3**, 1–28.
22. A. B. Kuznetsov, V. A. Melezhik, I. M. Gorokhov, N. N. Melnikov, G. V. Konstantinova, E. P. Kutyavin, and T. L. Turchenko, *Precambrian Res.*, 2010, **182**, 300–312. <https://doi.org/10.1016/j.precamres.2010.05.006>
23. H.-C. Chao, C.-F. You, H.-C. Liu, and C.-H. Chung, *Geochim. Cosmochim. Acta*, 2015, **165**, 324–341. <https://doi.org/10.1016/j.gca.2015.06.006>
24. G. F. de Souza, B. C. Reynolds, M. Kiczka, and B. Bourdon, *Geochim. Cosmochim. Acta*, 2010, **74**, 2596–2614. <https://doi.org/10.1016/j.gca.2010.02.012>
25. K. Luo, J. Ma, Z. Wang, G. Zhu, T. Zeng, and G. Wei, *Geochem. Geophys. Geosyst.*, 2024, **25**, e2023GC011215. <https://doi.org/10.1029/2023GC011215>
26. J. Brazier, A. Schmitt, E. Pelt, D. Lemarchand, S. Gangloff, T. Tacaïl, and V. Balter, *Geostand. Geoanal. Res.*, 2020, **44**, 331–348. <https://doi.org/10.1111/ggr.12308>

27. L. Yang, *Mass Spectrom. Rev.*, 2009, **28**, 990–1011. <https://doi.org/10.1002/mas.20251>
28. J. Meija, L. Yang, Z. Mester, and R. E. Sturgeon, *Isotopic Analysis – Fundamentals and Applications Using ICP-MS*, Wiley-VCH Verlag GmbH & Co., Weinheim, 2012, 113–137. <https://doi.org/10.1002/9783527650484.ch5>
29. A. Tchaikovskiy, B. Tobias, M. Berner, D. Pany-Kucera, P. Ingrová, Z. Hofmanová, T. Scharl, W. Pohl, and S. Hann, *Anal. Chim. Acta*, 2026, **1381**, 344783. <https://doi.org/10.1016/j.aca.2025.344783>
30. A. Ando, T. Okai, Y. Inouchi, and T. Igarashi, *Bull. Geol. Surv. Jpn.*, 1990, **41**, 27–48. https://www.gsj.jp/data/bull-gsj/41-01_02.pdf
31. Y. V. Erban Kochergina, V. Erban, and J. M. Hora, *J. Geosci.*, 2022, **67**, 273–285. <https://doi.org/10.3190/jgeosci.357>
32. A. Yu. Kramchaninov, I. V. Chernyshev, and K. N. Shatagin, *J. Anal. Chem.*, 2012, **67**, 1084–1092. <https://doi.org/10.1134/S1061934812140067>
33. T. Ohno and T. Hirata, *Anal. Sci.*, 2007, **23**, 1275–1280. <https://doi.org/10.2116/analsci.23.1275>
34. J. A. Stammeier, O. Nebel, D. Hippler, and M. Dietzel, *MethodsX*, 2020, **7**, 100847. <https://doi.org/10.1016/j.mex.2020.100847>
35. N. Sun, X.-Q. Chen, L.-L. Tian, and F. Huang, *J. Anal. At. Spectrom.*, 2022, **37**, 390–398. <https://doi.org/10.1039/D1JA00400J>
36. Aizawa S. and Akaiwa H., *Geochem. J.*, 1989, **23**, 69–75. <https://doi.org/10.14934/chikyukagaku.23.69>
37. W. Liu, H. Cai, W. Yuan, H. Zhou, and J. Chen, *J. Anal. At. Spectrom.*, 2025, **40**, 1977–1984. <https://doi.org/10.1039/D5JA00165J>
38. Y. Kirichenko, J. D. Rickli, T. R. R. Bontognali, and N. Shalev, *Geochim. Cosmochim. Acta*, 2024, **378**, 270–285. <https://doi.org/10.1016/j.gca.2024.06.006>
39. M. J. Kim and S.-G. Lee, *Korean J. Mineral. Petrol.*, 2022, **35**, 507–520. <https://doi.org/10.22807/KJMP.2022.35.4.507>
40. J. R. De Laeter, J. K. Böhlke, P. De Bièvre, H. Hidaka, H. S. Peiser, K. J. R. Rosman, and P. D. P. Taylor, *Pure Appl. Chem.*, 2003, **75**, 683–800. <https://doi.org/10.1351/pac200375060683>
41. J. Wang, Y. Di, D. Asael, N. J. Planavsky, and L. G. Tarhan, *Chem. Geol.*, 2023, **621**, 121365. <https://doi.org/10.1016/j.chemgeo.2023.121365>
42. C. T. Gerritzen, S. Goderis, H. F. James, and C. Snoeck, *Spectrochim. Acta B*, 2024, **217**, 106955. <https://doi.org/10.1016/j.sab.2024.106955>
43. H.-C. Liu, C.-F. You, K.-F. Huang, and C.-H. Chung, *Talanta*, 2012, **88**, 338–344. <https://doi.org/10.1016/j.talanta.2011.10.050>
44. L. Yang, C. Peter, U. Panne, and R. E. Sturgeon, *J. Anal. At. Spectrom.*, 2008, **23**, 1269–1274. <https://doi.org/10.1039/b803143f>
45. D. Guiserix, E. Albalat, H. Ueckermann, P. Davechand, L. M. Iaccheri, G. Bybee, S. Badenhorst, and V. Balter, *Chem. Geol.*, 2022, **606**, 121000. <https://doi.org/10.1016/j.chemgeo.2022.121000>
46. J. Irrgeher, T. Prohaska, R. E. Sturgeon, Z. Mester, and L. Yang, *Anal. Methods*, 2013, **5**, 1687–1694. <https://doi.org/10.1039/c3ay00028a>
47. Y. Hu and F.-Z. Teng, *J. Anal. At. Spectrom.*, 2019, **34**, 338–346. <https://doi.org/10.1039/C8JA00335A>
48. J. Xu, S. Yang, Y. Yang, Y. Liu, and X. Xie, *Atom. Spectrosc.*, 2020, **41**, 64–73. <https://doi.org/10.46770/AS.2020.02.003>
49. Y.-H. Yang, F.-Y. Wu, L.-W. Xie, J.-H. Yang, and Y.-B. Zhang, *Spectrochim. Acta B*, 2011, **66**, 656–660. <https://doi.org/10.1016/j.sab.2011.07.004>
50. H. Wierzbowski, R. Anczkiewicz, J. Bazarnik, and J. Pawlak, *Chem. Geol.*, 2012, **334**, 171–181. <https://doi.org/10.1016/j.chemgeo.2012.10.019>
51. Y.-B. Lin, H.-Z. Wei, S.-Y. Jiang, S. Hohl, H.-L. Lei, X. Liu, and G. Dong, *Anal. Chem.*, 2020, **92**, 2417–2424. <https://doi.org/10.1021/acs.analchem.9b03137>
52. K. Wu, Y. Ueno, J. Surma, and C. Nakajo, *Geostand. Geoanal. Res.*, 2025, **49**, 751–769. <https://doi.org/10.1111/ggr.70002>
53. N. Wu, J. Zhang, H. Mao, G. Zhang, and Z. Zhao, *Geosyst. Geoenviron.*, 2024, **3**, 100144. <https://doi.org/10.1016/j.geogeo.2022.100144>
54. N. Su, S. Yang, K. Deng, Y.-P. Chang, J. Xu, and Z. Wu, *Earth Planet. Sci. Lett.*, 2021, **576**, 117235. <https://doi.org/10.1016/j.epsl.2021.117235>
55. E. I. Stevenson, S. M. Aciego, P. Chutcharavan, I. J. Parkinson, K. W. Burton, M. A. Blakowski, and C. A. Arendt, *Chem. Geol.*, 2016, **429**, 33–43. <https://doi.org/10.1016/j.chemgeo.2016.03.008>
56. S. Bang and Y. I. Lee, *Palaeogeogr. Palaeoclimatol. Palaeoecol.*, 2020, **541**, 109534. <https://doi.org/10.1016/j.palaeo.2019.109534>
57. J. Jeong, S. Bang, D. J. Wilson, and Y. Huh, *Chem. Geol.*, 2025, **690**, 122859. <https://doi.org/10.1016/j.chemgeo.2025.122859>
58. P. A. E. Pogge von Strandmann, D. N. Schmidt, N. J. Planavsky, G. Wei, C. L. C. Jones, and K.-H. Baumann, *Chem. Geol.*, 2019, **530**, 119338. <https://doi.org/10.1016/j.chemgeo.2019.119338>
59. A. Yu. Kramchaninov, *J. Anal. Chem.*, 2021, **76**, 1549–1557. <https://doi.org/10.1134/S1061934821130062>